

ECE 214 DC to DC Converter

Labs 7, 8, 9 and 10

Landyn Francis
Jacob Mealey

April 29, 2021

Abstract

The design, simulation, and construction of a 12 to 25V DC to DC Converter is described. The circuit specifications called for an output voltage of $25 \pm 0.25V$, with an AC ripple of less than $0.5mV_{pp}$. The final circuit performed to specifications, producing an output voltage of $25.0V$, with an AC ripple of $476.49\mu V_{pp}$ at a frequency of $22.864kHz$. An astable multivibrator circuit was used to drive a boost converter circuit which increased the voltage. The output of the boost converter was then attenuated by a RC low pass filter, in order to bring the AC ripple within specifications.

Contents

List of Figures	iv
List of Tables	vi
1 Introduction	1
2 Circuit Design and Analysis	2
2.1 Boost Converter Circuit and Analysis	3
2.1.1 Calculation of Energy Loss in the Capacitor	3
2.1.2 Calculation of Time for Current to Flow Into the Inductor	4
2.1.3 Calculation of Time for Current to Flow Out of the Inductor	4
2.1.4 Calculation and Selection of Output Resistor	5
2.1.5 Calculation of Waveform Generator Settings	5
2.2 Astable Multivibrator Circuit and Analysis	5
2.2.1 Calculation of Frequency	6
2.2.2 Selection of Capacitor Values	7
2.3 Low Pass Filter Circuit and Analysis	7
2.4 Thevenin Equivalent Output Impedance of the DC–DC Power Supply	8
3 Simulated Performance	14
3.1 Boost Converter Simulation	15
3.1.1 Transient Analysis	15
3.1.2 Current through Transistor	16
3.1.3 Temperature Analysis	16
3.2 Astable Multivibrator Simulation	17
3.2.1 Tuning the Simulation Results	17
3.2.2 Simulating the Final Circuit	19
3.2.3 Capacitor and Resistor Sensitivity Analysis	19
3.3 DC–DC Power Supply Simulation	22
4 Experimental Implementation	23
4.1 Boost Converter	24
4.2 Astable Multivibrator	25
4.2.1 Determining 2N7000 Trigger Voltage	26
4.2.2 Driving the Boost Converter	28
4.2.3 Checking the IRFD110 Transistor	29
4.3 DC–DC Power Supply	30
5 Discussion	31
5.1 Boost Converter	32
5.2 Astable Multivibrator	32
5.3 Low Pass Filter	33
5.4 DC–DC Power Supply	34
6 DC–DC Power Supply Cost Estimate	34

7	Conclusions	36
	Appendices	37
A	Bill of Materials	37
	References	38

List of Figures

1	Block diagram of the DC–DC power supply(taken from ECE214 Lab 9 instructions [1]).	2
2	Basic layout for the three circuits of the DC–DC Power Supply.	2
3	Boost converter circuit using ideal switches.	3
4	Astable multivibrator as simulated with C_1 and C_2 equal to $0.1\mu\text{F}$	6
5	Low pass filter ideal schematic.	8
6	Power supply schematic in State 1.	9
7	Thevenin equivalent magnitude in state 1	9
8	Thevenin equivalent phase angle in state 1	10
9	Thevenin equivalent resistance in state 1	10
10	Thevenin equivalent reactance in state 1	11
11	Power supply schematic in state 2	11
12	Thevenin equivalent magnitude in state 2	12
13	Thevenin equivalent phase angle in state 2	12
14	Thevenin equivalent resistance in state 2	13
15	Thevenin equivalent reactance in state 2	13
16	Thevenin equivalent circuit for the DC–DC power supply.	14
17	Power supply circuit as simulated.	14
18	Boost converter circuit as simulated.	15
19	Transient simulations for boost converter output voltage.	15
20	Transient simulations for boost converter current through transistor.	16
21	Temperature analysis over the range $-20^\circ\text{C} - 60^\circ\text{C}$	16
22	Astable multivibrator as simulated.	17
23	Simulations run at C_1 and C_2 equal to $0.1\mu\text{F}$, before V_{t0} was adjusted.	18
24	Simulations run at C_1 and C_2 equal to $0.1\mu\text{F}$, after V_{t0} was adjusted.	18
25	Transient simulation run with final capacitor values C_1 equal to 498pF and C_2 equal to 706pF	19
26	Component sensitivity analysis simulations ran for C_1	20
27	Component sensitivity analysis simulations ran for C_2	20
28	Component sensitivity analysis simulations ran for R_x	21
29	Component sensitivity analysis simulations ran for R_d	21
30	Component sensitivity analysis simulations ran for R_u	22
31	Power supply circuit as simulated.	22
32	Transient Analysis Simulations of the DC–DC power supply.	23
33	Final schematic of DC–DC power supply, as measured.	23
34	Final schematic of boost converter circuit.	24
35	Measurements of boost converter circuit.	25
36	Picture of the circuit including DVM measurements.	25
37	Astable Multivibrator as measured.	26
38	Astable Multivibrator half circuit.	26
39	Measurement of V_{t0} for transistors 1 and 2.	27
40	Measurement of V_{t0} for transistor 3.	27
41	Measurement of Frequency with C_1 and C_2 equal to $0.1\mu\text{F}$	28
42	Measurements taken of combined boost converter and astable multivibrator circuits.	28
43	Photo of combined boost converter and astable multivibrator circuits.	29

44	Measurement taken across the 1Ω resistor in the boost converter circuit.	29
45	Final schematic of DC–DC power supply, as measured.	30
46	Measurement of AC ripple across the load resistor.	30
47	Photo of DVM measuring across the load resistor.	31

List of Tables

I	Boost converter comparisons.	32
II	Astable multivibrator comparisons.	33
III	Low pass filter comparisons.	33
IV	DC–DC power supply comparisons	34
V	DC–DC power supply cost estimate	35
VI	Bill of materials for 1 DC–DC power supply.	37

1 Introduction

This report details the design, simulation, and construction of a 12 to 25 V DC to DC converter. The converter consists of a boost converter circuit, an astable multivibrator circuit, and a low pass filter. The boost converter circuit increases the DC voltage from 12 to 25V DC. This is accomplished by transferring energy out of an inductor into a capacitor, at the same rate the energy is lost from the capacitor. The output voltage was controlled by changing how long the energy is allowed to flow out of the inductor into the capacitor.

Boost converters are generally used to increase a DC voltage signal, as indicated by their alternate name, the step up converter. This was useful to the power supply because it accomplished the primary objective of the power supply, raising the voltage from 12 to 25V DC. However, the boost converter as designed required a waveform to control the voltage controlled switches. These switches regulated the energy leaving the inductor. In one state, they allowed the energy to flow to the capacitor, and in the other state they did not. In order to control these switches, a square wave signal with a specific frequency and duty cycle was required. The astable multivibrator accomplished this task.

An astable multivibrator is a relaxation circuit, one capacitor at a time was perturbed, then allowed to return to its steady state. When the voltage across the first capacitor crossed the threshold of its own voltage controlled switches, the other capacitor was perturbed and the cycle began again. One side of each capacitor produces the same square wave signal, at a 180° phase shift, relative to the other. By changing the two capacitor values, this square wave's frequency and duty cycle could be changed to properly drive the boost converter to output 25V DC. Astable multivibrators are generally used to create a square wave with a controllable frequency and duty cycle. This has a wide range of uses from radio signals to analog integrated circuits.

Finally, the output of the boost converter was sent through a RC low pass filter. This was a standard third order RC low pass filter which attenuated all signals at frequencies higher than the cutoff frequency. The cutoff frequency is related to the capacitor and resistor values present in the filter. The boost converter output was filtered to remove the AC ripple signal that was present on the 25V DC output signal. Low pass filters can be used in almost any circuit that needs to attenuate frequencies past a predetermined frequency. The circuit must produce a 25 ± 0.25 V DC signal across a $10\text{k}\Omega$ resistive load, with an input of 12 V DC. The AC Ripple on the output must be no greater than $0.10\text{mV}_{\text{PP}}$. Section 2 of this report describes the calculation and design of the component values for the circuits in the DC–DC power supply. Simulation results are shown in Section 3, and the experimental results in Section 4. The results of the circuit are discussed in Section 5. A cost analysis is provided in Section 6, and conclusions are presented in Section 7.

2 Circuit Design and Analysis

Figure 1 shows the block diagram of the DC–DC power supply.

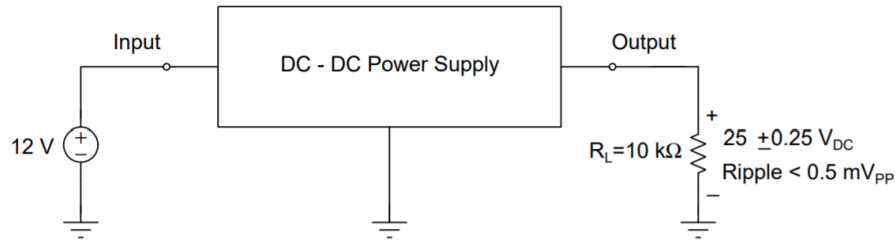


Fig. 1. Block diagram of the DC–DC power supply(taken from ECE214 Lab 9 instructions [1]).

As can be seen in Figure 1, the specifications for the output voltage were as follows: The DC output voltage must be $25 \pm 0.25\text{V}$, with an AC ripple of less than 0.5mV_{PP} . The power supply works by combining three independent circuits together. The increase of voltage is handled by the boost converter, which is driven by the astable multivibrator. The low pass filter attenuates the AC ripple present on the output of the boost converter. The boost converter operates by transferring energy from an inductor to a capacitor at regular intervals in order to boost the voltage across the capacitor. The circuit used an IRFD110 metal–oxide semiconductive field–effect transistor (MOSFET) as a voltage controlled switch. This switch was controlled by the astable multivibrator circuit, thus controlling the output voltage of the boost converter. The output of the boost converter was then filtered by the low pass filter to reduce AC ripple. Figure 2 shows how the three circuits are connected.

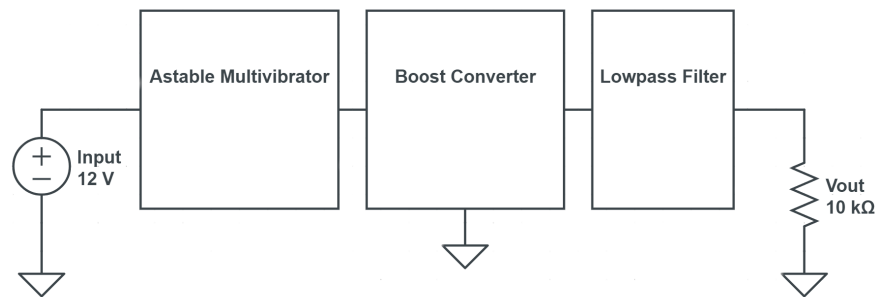


Fig. 2. Basic layout for the three circuits of the DC–DC Power Supply.

As can be seen in Figure 2, the astable multivibrator and boost converter both took 12V DC as input. The boost converter also took the output of the astable multivibrator as an input. Lastly, the low pass filter takes the output of the boost converter as its input, and outputs the final voltage signal. Sections 2.1, 2.2, and 2.3 discuss the design of the boost converter, astable multivibrator, and low pass filter, respectively.

Section 2.4 shows the calculations to find the Thevenin Equivalent Circuit of the power supply.

2.1 Boost Converter Circuit and Analysis

The boost circuit shown in Figure 3 was used to increase the DC voltage from 12 V to 25 V.

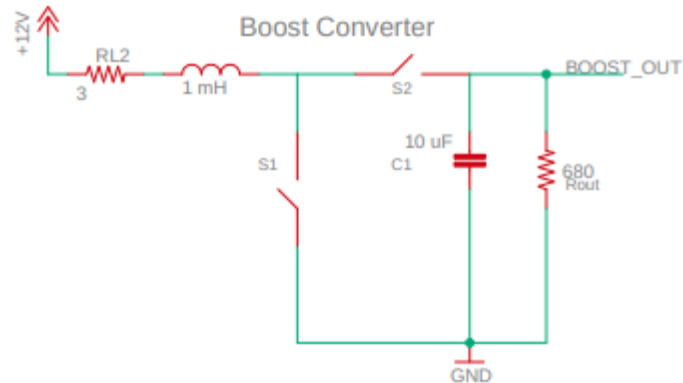


Fig. 3. Boost converter circuit using ideal switches.

As can also be seen in Figure 3, the boost circuit features an inductor and a capacitor, the values for these components were predetermined as 1mH and 10uF respectively. Additionally, there are two synchronized switches S_1 and S_2 , these switches cannot be open or closed at the same time. If S_1 is open, S_2 must be closed, and vice versa. In order to increase the DC voltage from 12V to 25V, the energy lost in the capacitor must be equal to the energy stored in the inductor. The circuit reaches a steady state when the energy transferred from the inductor to the capacitor. When switch S_1 is open and switch S_2 is closed, is equal to the energy lost from the capacitor. When switch S_1 is closed and switch S_2 is open.

2.1.1 Calculation of Energy Loss in the Capacitor

The boost converter operates by transferring energy between an inductor and a capacitor at a rate equal to the energy loss in the capacitor. Therefore, the energy lost by the capacitor must first be calculated. The energy stored in a capacitor is defined by Equation 1.

$$E_c = \frac{1}{2} C \cdot V_c(t) \quad (1)$$

Here, $V_c(t)$ is the voltage across the capacitor as a function of time. The change in energy was calculated with Equation 2.

$$\Delta E_c = \frac{1}{2} C (V_1^2 - V_2^2) \quad (2)$$

With C equal to $10\mu F$, V_1 equal to $25.05V$ and V_2 equal to $24.95V$, the change of energy stored in the capacitor can be directly calculated. Plugging these values into Equation 2 resulted in ΔE_C equalling $25\mu J$.

2.1.2 Calculation of Time for Current to Flow Into the Inductor

Next, the time for the current to flow into inductor must be calculated. This value is defined as t_1 . Energy stored in the inductor is defined by in Equation 3, the current can be solved for by substituting E_L for ΔE_c found in Equation 2 and L equal to $1mH$, resulting in i_L equalling $223mA$.

$$E_L = \frac{1}{2} \cdot L \cdot i_L(t)^2 = 25\mu J \quad (3)$$

When S_1 is closed, $i_L(t)$ is defined in Equation 4. When setting $i_L(t)$ to $223mA$ and L equal to $10mH$, t_1 can be solved for, equalling $18.58\mu s$.

$$i_L(t) = \frac{12}{L}t \quad (4)$$

2.1.3 Calculation of Time for Current to Flow Out of the Inductor

Next, the time for current to flow out of the inductor into the capacitor must be calculated. This value is defined as t_2 . To solve for t_2 , i_L must be calculated when S_1 open is and S_2 is closed, Equation 5, the current for a series RLC circuit must be used. A_1 and A_2 are simply coefficients in the RLC current equation.

$$i(t) = A_1 e^{-\alpha t} \cos(\omega_d t) + A_2 e^{-\alpha t} \sin(\omega_d t) \quad (5)$$

The constants in Equation 5 are defined as follows: Neper frequency (α) in Equation 6, Resonant frequency (ω_0) in Equation 7, and damped resonant frequency (ω_d) in Equation 8. As seen in Equations 6 and 7, the Neper frequency is less than the resonant frequency, the circuit is underdamped. $V_L(0^+)$ was determined by using Kirchhoff's Voltage Law around the circuit.

$$\alpha = \frac{R}{2L} = 1,500 \frac{rad}{s} \quad (6)$$

$$\omega_0 = \frac{1}{\sqrt{L \cdot C}} = 10,000 \frac{rad}{s} \quad (7)$$

$$\omega_d = \sqrt{\omega_0^2 - \alpha^2} = 9886.859 \frac{rad}{s} \quad (8)$$

$$A_1 = i(0) = .223 \quad (9)$$

$$A_2 = \frac{1}{\omega_d} \left[\frac{V_L(0^+)}{L} + \alpha \cdot i_0 \right] = -1.343 \quad (10)$$

When substituting these constants into Equation 5 and setting $i(t) = 0$, t_2 can be solved for, resulting in t_2 equalling $16.6 \mu s$

2.1.4 Calculation and Selection of Output Resistor

The output resistor is denoted as R_0 , which was calculated using Equation 11. Where τ is the time constant of the simple RC circuit, Equation 12. In that equation, R_0 is the output resistor, and C is a $10\mu F$ capacitor. Setting t equal to t_1 , which is equal to $18.58\mu s$, then setting $V_{out}(t)$ equal to $24.95V$ and $V_{out}(0)$ equal to $25.05V$ results in R_0 equal to 475Ω . However this was adjusted to 680Ω to reduce power dissipation.

$$V_{out}(t) = V_{out}(0)e^{\frac{-t}{\tau}} \quad (11)$$

$$\tau = R_0 \cdot C \quad (12)$$

Power dissipation was calculated by Equation 13 where P is Power, V is the Voltage across Resistor, and R is resistance.

$$P = \frac{V^2}{R} \quad (13)$$

Plugging in V equal to $25V$ and R equal to 680Ω , P equals $.919W$, indicating a resistor bank will be necessary to safely dissipate power, because the resistors given only have $0.25W$ of power dissipation.

2.1.5 Calculation of Waveform Generator Settings

The waveform generator calculations were straightforward, the pulse must be high for as long as t_1 and low for as long as t_2 . This results in the waveform generator outputting a square wave of period T , and a duty cycle of δ . When t_1 is equal to $18.58\mu s$, and t_2 is equal to $16.6\mu s$, T is given by Equation 14, resulting in T equalling $35.18\mu s$.

$$T = t_1 + t_2 \quad (14)$$

Using $35.18\mu s$ as T , and 18.58 as t_1 , the duty cycle is equal to Equation 15.

$$\delta = \frac{t_1}{T} = 52.896\% \quad (15)$$

2.2 Astable Multivibrator Circuit and Analysis

The astable multivibrator shown in Figure 4 was used to operate the voltage controlled switch in the boost converter.

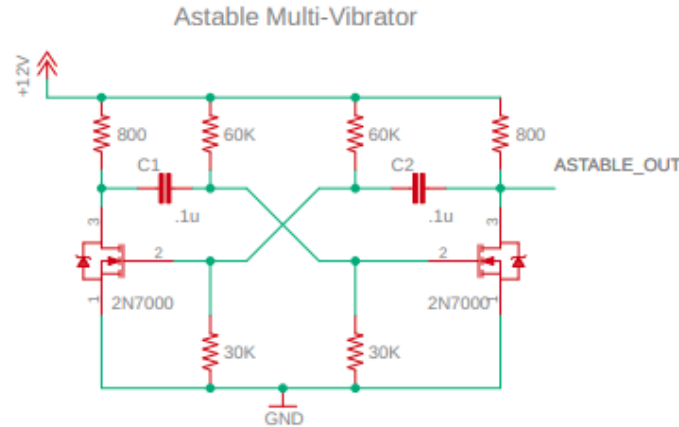


Fig. 4. Astable multivibrator as simulated with C_1 and C_2 equal to $0.1\mu\text{F}$.

As can be seen in Figure 4, the circuit used voltage controlled switches (2N7000 NPN transistors). The multivibrator works by raising the voltage on one side of either capacitor, which then starts to return to its steady state. Once it crosses the trigger voltage of the 2N7000's one side of the other capacitor is raised, repeating the process. The circuit operates in two states: Switch nearest the capacitor was open for a long time, then closed (State 1), or vice versa (State 2). The different states effect the time constants, which will be used in calculating frequency. The frequency and duty cycle of the output signal are determined by the capacitor values, C_1 and C_2 . The initial capacitor values were equal to $0.1\mu\text{F}$ and were later simulated and measured to confirm the accuracy of the simulations. After confirming simulation accuracy, the simulations could later be used for finding capacitor values.

2.2.1 Calculation of Frequency

Frequency and duty cycle control the boost converter. Frequency was easily calculated, while duty cycle was determined by simulation and measurement results in Sections 3.2 and 4.2 respectively. To calculate the frequency of the astable multivibrator output, two nonlinear equations are given:

$$V_c(t) = V_c(\infty) + [13.5 - V_c(\infty)]e^{-t/\tau_2} \quad (16)$$

$$V_c(t) = V_c(\infty) + [(V_x - 12) - V_c(\infty)]e^{-(t-\frac{T}{2})/\tau_1} \quad (17)$$

If t is equal to $\frac{T}{2}$ and T , Equations 18 and 19 are derived.

$$V_x = V_c(\infty) + [13.5 - V_c(\infty)]e^{-T/2\tau_2} \quad (18)$$

$$1.5 = V_c(\infty) + [(V_x - 12) - V_c(\infty)]e^{-\frac{T}{2\tau_1}} \quad (19)$$

Here, T is period and τ_1 and τ_2 are time constants that relate to each half of the circuit. V_x is the voltage at which the circuit switches states. 1.5V is the trigger voltage of the NP7000 Transistors used, which is

also the other point where the circuit switches state. Because the 30k Ω and 60k Ω resistors act as a voltage divider on the 12V source, $V_c(\infty)$ in Equations 18 and 19 was calculated by the equation:

$$V_c(\infty) = 12\left(\frac{R_1}{R_1 + R_2}\right) \quad (20)$$

This yields $V_c(\infty)$ equal to 4. Next, to find the values of τ_1 and τ_2 , Equation 21 was used.

$$\tau = R \cdot C \quad (21)$$

τ_1 and τ_2 are defined as the time constant for each state. Here, R is equal to R_1 in parallel with R_2 in State 1, and equal to R_3 in series with the parallel combination of R_1 and R_2 in State 2, thus resulting in τ_1 equalling 2ms and τ_2 equalling 2.08ms. This equation is shown in the following two equations.

$$\tau_1 = R \cdot C \quad (22)$$

$$\tau_2 = R \cdot C \quad (23)$$

Plugging $V_c(\infty)$, τ_1 , and τ_2 into Equations 18 and 19 yields:

$$4 + [13.5 - 4]e^{-T/2.00208} = V_x \quad (24)$$

$$4 + [(V_x - 12) - 4]e^{-\frac{T}{2.002}} = 1.5 \quad (25)$$

Finally, solving for V_x and T yields V_x equal to 6.68V and T equal to 5.26ms. Frequency was derived from the period using the following equation.

$$f = 1/T \quad (26)$$

This results in a final calculated frequency of f equal to 190Hz.

2.2.2 Selection of Capacitor Values

Capacitor values were selected by tuning the simulation to measured values by changing the V_{t0} value for the simulated transistors to the ones measured. The simulation process is described in Section 3.2, and the measurement process is described in Section 4.2. Ultimately, the process ended in a selection of C_1 equal to 498pF, and C_2 equal to 706pF.

2.3 Low Pass Filter Circuit and Analysis

Figure 5 shows the schematic for a third order low pass filter.

Low Pass Filter

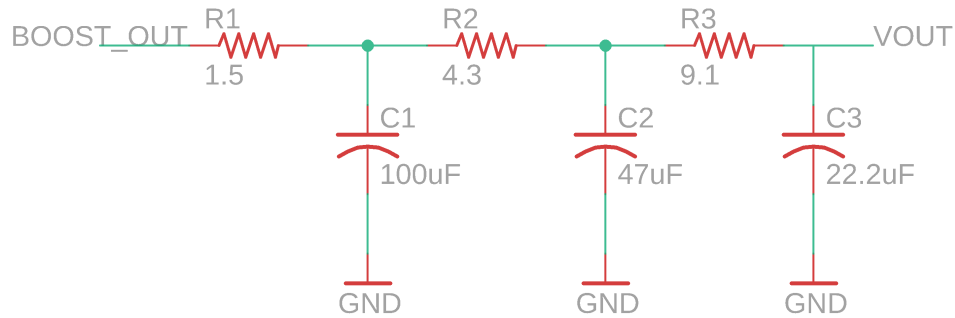


Fig. 5. Low pass filter ideal schematic.

Calculations were relatively short for the low pass filter because the frequency of the AC ripple was already known. It was predicted that a third order filter would be needed. The values for the three resistors and capacitors are governed by the following equations.

$$C_1 \gg C_2 \gg C_3 \quad (27)$$

$$R_3 \gg R_2 \gg R_1 \quad (28)$$

$$R_1 C_1 = R_2 C_2 = R_3 C_3 \quad (29)$$

Equations 27 and 28 ensure that individual filter stages do not load the previous stages. It was found that Equation 29 was not strictly necessary for the filter to work. Equation 29 only ensures that each stage has the same cutoff frequency, defined by Equation 30.

$$f_c = \frac{1}{2 \cdot \pi \cdot R \cdot C} \quad (30)$$

It was known that the DC voltage is at a frequency of 0Hz, and the AC ripple had a frequency of approximately 23kHz. Therefore, a low cutoff frequency was needed to sufficiently attenuate the AC ripple, while leaving the DC signal unaffected. It was also known that high resistor values would reduce the DC signal significantly, so large capacitors were appropriate. Due to part availability C_1 , C_2 , and C_3 were determined to be $100\mu\text{F}$, $47\mu\text{F}$, and $22.2\mu\text{F}$. Setting f_c to 500Hz, and plugging in C_1 , C_2 , and C_3 one at a time into Equation 30 resulted in: R_1 , R_2 , and R_3 equal to 3.2Ω , 6.4Ω , 12.8Ω respectively. For part availability, those values were changed to 3.3Ω , 6.2Ω , and 12Ω . With these adjusted values, the new calculated cutoff frequencies f_{c1} , f_{c2} , f_{c3} were equal to 482, 546, and 597Hz, respectively.

2.4 Thevenin Equivalent Output Impedance of the DC-DC Power Supply

The Thevenin equivalent circuit was also investigated to observe the circuit's behavior at the output. The open circuit voltage V_{oc} , was known to be 25V DC. Calculating the Thevenin equivalent impedance involved investigating two states of the circuit. State 1 was when switch S_1 in the boost converter is closed

and S_2 is open. State 2 was the opposite, S_1 is open, and S_2 is closed. Figure 6 shows the circuit schematic for state 1.

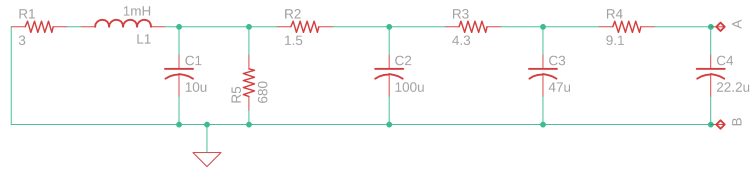


Fig. 6. Power supply schematic in State 1.

First, the circuit was then converted to phasor form, using the next two equations:

$$Z_c(f) = \frac{-j}{(2 \cdot \pi \cdot f) \cdot C} \quad (31)$$

$$Z_l(f) = j \cdot (2 \cdot \pi \cdot f) \cdot L \quad (32)$$

After the circuit was in phasor form, the impedances were combined to arrive at an equation in terms of f , frequency. This equation was determined inside Matlab, and is too long to display here. Instead, the 4 components of the impedance (magnitude, phase angle, resistance and reactance) were plotted as a function of frequency, f . Figure 7 shows the magnitude vs. frequency plot.

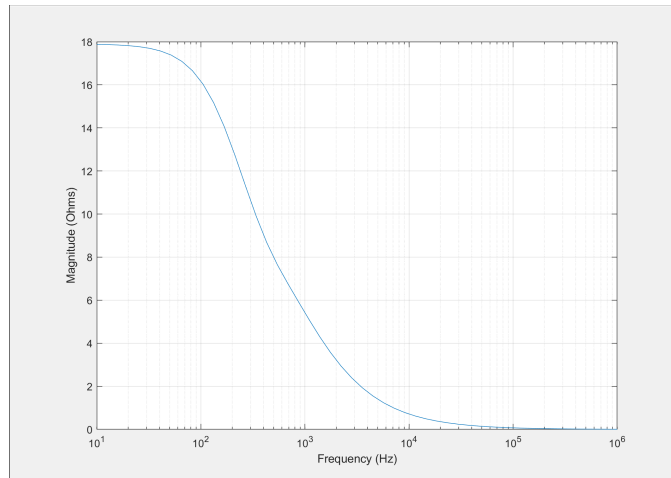


Fig. 7. Thevenin equivalent magnitude in state 1

Figure 8 shows the phase angle vs. frequency plot.

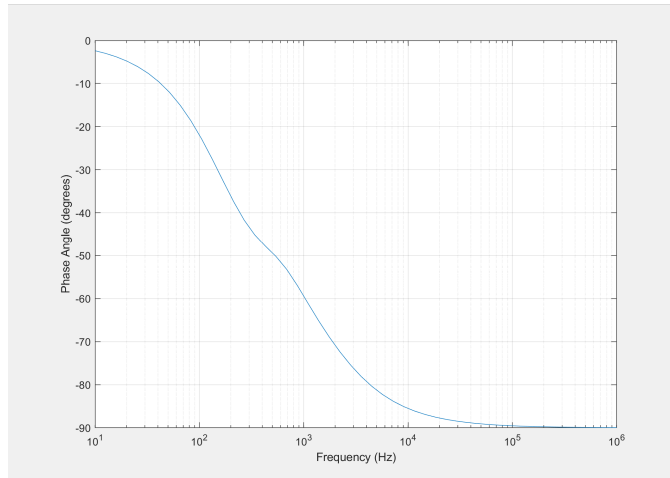


Fig. 8. Thevenin equivalent phase angle in state 1

Figure 9 shows the real part (resistance) of the impedance as a function of frequency.

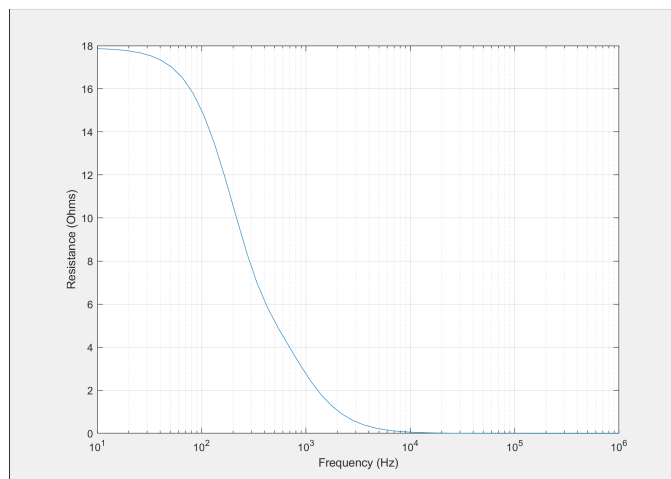


Fig. 9. Thevenin equivalent resistance in state 1

Figure 10 shows the imaginary part (reactance) of the impedance as a function of frequency.

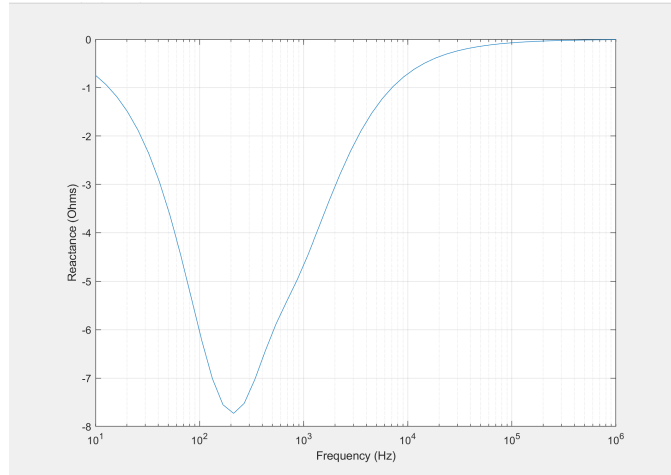


Fig. 10. Thevenin equivalent reactance in state 1

The equivalent impedance components vary widely at different frequencies, this was attributed to the inductor being present in State 1 and not in State 2. Next, the Thevenin equivalent impedance was found for state 2. Figure 11 shows the circuit schematic for state 2.

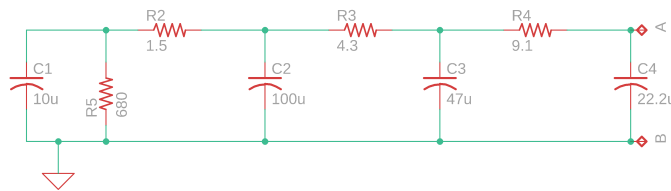


Fig. 11. Power supply schematic in state 2

The circuit was again converted to phasor form using Equations 31 and 32. The process for state 2 was the same as for state 1, resulting in plots for each component of the equivalent impedance as well. Figure 12 shows the magnitude vs. frequency plot.

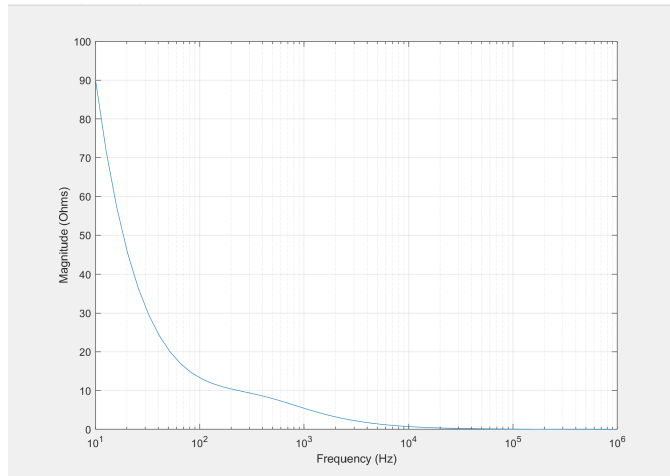


Fig. 12. Thevenin equivalent magnitude in state 2

Figure 13 shows the phase angle vs. frequency plot.

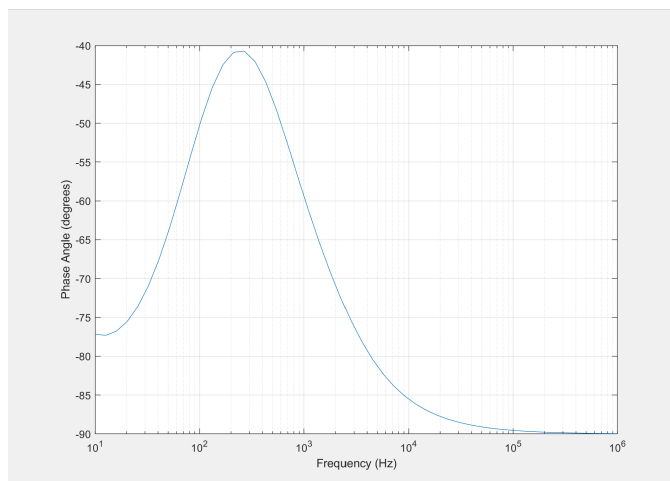


Fig. 13. Thevenin equivalent phase angle in state 2

Figure 14 shows the real part (resistance) of the impedance as a function of frequency.

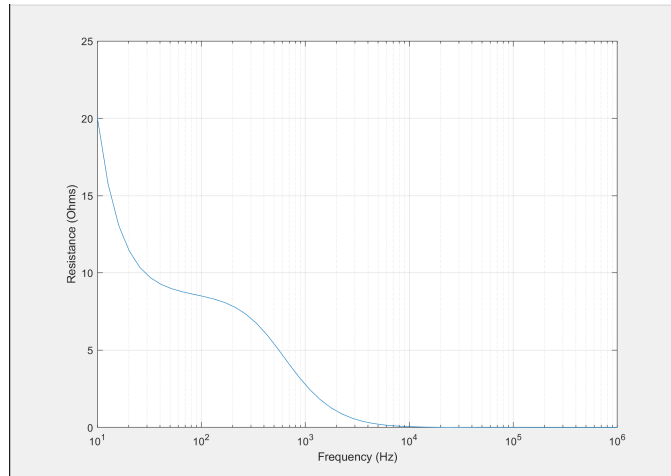


Fig. 14. Thevenin equivalent resistance in state 2

Figure 15 shows the imaginary part (reactance) of the impedance as a function of frequency.

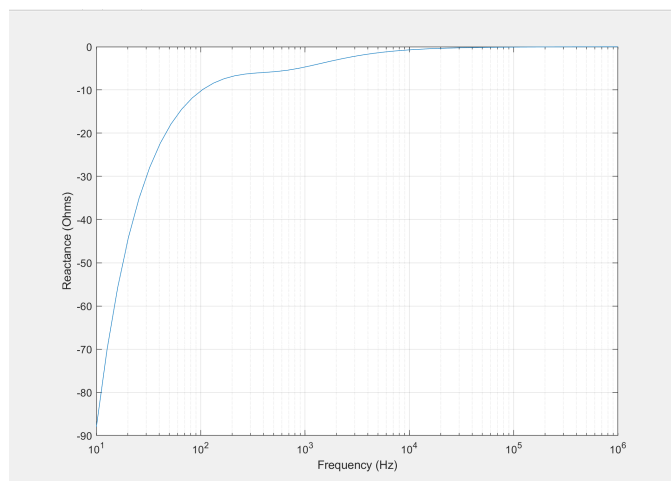


Fig. 15. Thevenin equivalent reactance in state 2

Both equivalent impedances were a function of frequency, so the astable multivibrators frequency of approximately 23kHz was used to draw the Thevenin circuit. Initially, the equivalence of the two impedances at 23kHz was questioned, however upon further consideration, this made sense. The circuit operates at roughly 23k, and is constantly switching between states S_1 and S_2 . Therefore, it would be bad design if at the operating frequency, the Thevenin equivalent impedance, and by extension the power delivered to the load was changing significantly. Figure 16 shows the final Thevenin equivalent circuit.

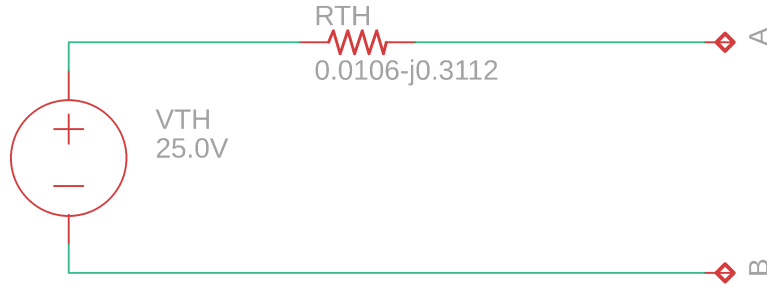


Fig. 16. Thevenin equivalent circuit for the DC-DC power supply.

Here, R_{TH} is the Thevenin equivalent impedance at f equal to 23kHz for both state 1 and 2. As mentioned above, these were the same value at this specific frequency.

3 Simulated Performance

Figure 17 shows the final power supply circuit as simulated.

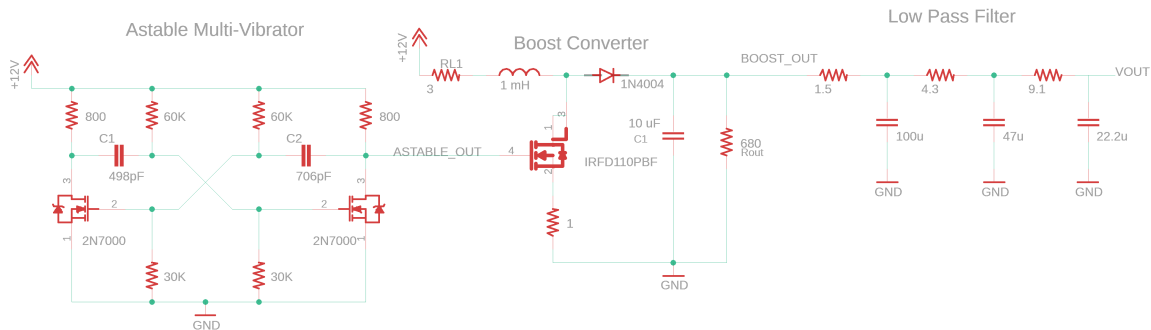


Fig. 17. Power supply circuit as simulated.

A more in depth explanation of this simulation can be found in Section 3.2.2. Simulations were vitally important for effectively designing each circuit. They provided a check for previous calculations and also helped determine values for the multivibrator. Simulations were run using NGSpice, Sue2, and MatLab. Calculated values were often changed to account for the difference between real and ideal components and to ensure all specifications were met. Sections 3.1, 3.2, and 3.3 discuss the simulations for the boost converter, astable multivibrator, and full power supply, respectively.

3.1 Boost Converter Simulation

Figure 18 shows the boost converter schematic on which simulations were performed, with the AD2 Wavegen driving the switches.

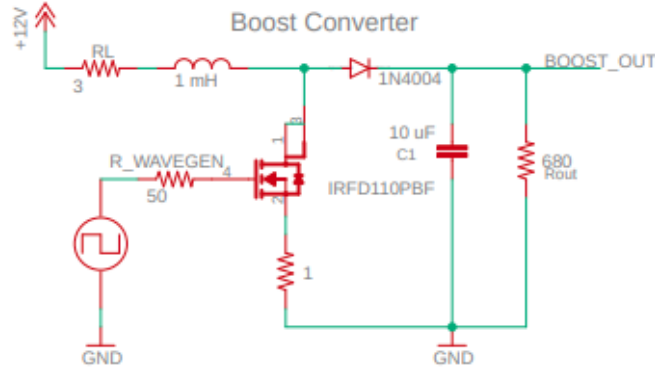


Fig. 18. Boost converter circuit as simulated.

The boost converter circuit shown in figure 18 was simulated to inspect two components: the voltage across the output resistor (to match design requirements), as well as the current through the transistor which had a maximum current of 600mA , as specified Table VI, shown in Section A. From the simulations, a new period and a duty cycle were chosen, T was equal to $40\mu\text{s}$ and δ equal to 54.76%

3.1.1 Transient Analysis

The output voltage was confirmed at 25V DC shown in Figure 19a, which meets circuit specifications. The ripple was also observed, as seen in Figure 19b, measuring $.0989\text{V}$ Peak to Peak. This was approximately 1V above the specification for the final circuit, but was later reduced by the low-pass filter.

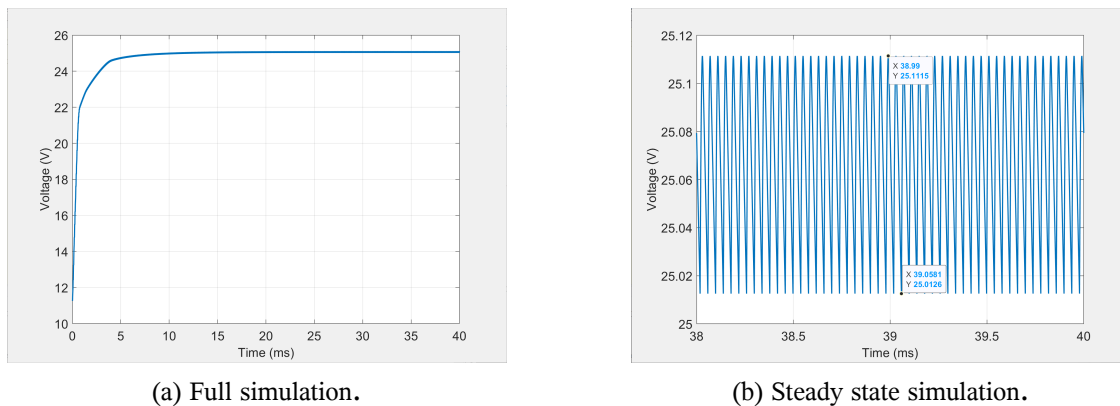


Fig. 19. Transient simulations for boost converter output voltage.

3.1.2 Current through Transistor

The Metal–Oxide–Semiconductor Field–Effect Transistors (MOSFETs) used were IRFD110's which have a maximum current of 600mA . To ensure this current was never exceeded, simulations were run on a 1Ω resistor connected in series to the transistor. The voltage across this resistor was simulated, and from there, the current was found. Figure 20a shows that the simulated current through the MOSFET never exceeded 449mA . Figure 20b shows the steady state current was also safe for the IRFD110.

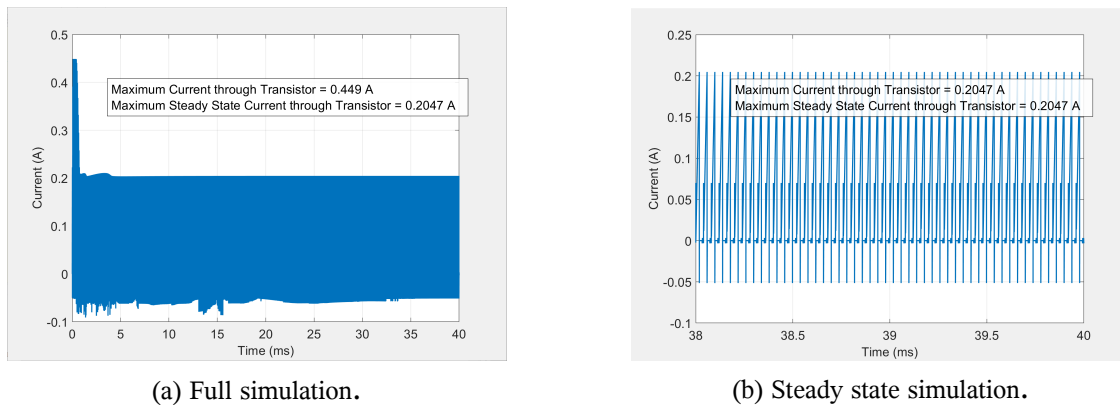


Fig. 20. Transient simulations for boost converter current through transistor.

As can be seen in Figure 20, the current was safe for the IRFD110 throughout the entire simulation.

3.1.3 Temperature Analysis

Due to the temperature dependence of resistors, a simulation of the circuit performance was run over a wide range of temperatures, the results of which can be seen in Figure 21.

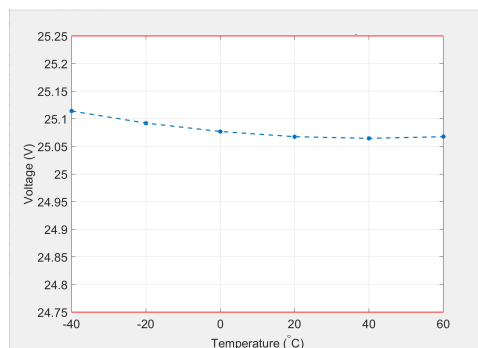


Fig. 21. Temperature analysis over the range -20°C – 60°C .

There was little variation at different temperatures, as was expected with the metal–film resistors used.

Metal–film resistors have a temperature coefficient of resistance (TCR) of only +70ppm per C°, therefore they are not heavily affected by temperature change.

3.2 Astable Multivibrator Simulation

Simulations were used to determine the capacitor values of the astable multivibrator shown in Figure 22.

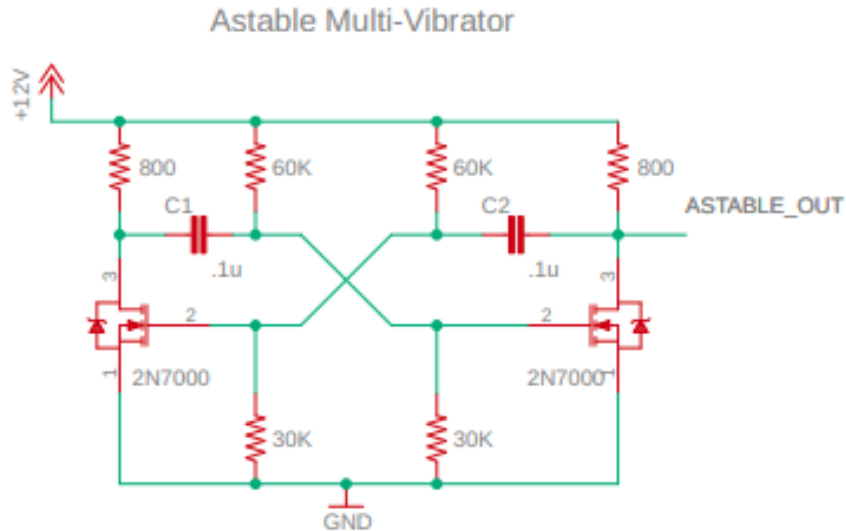
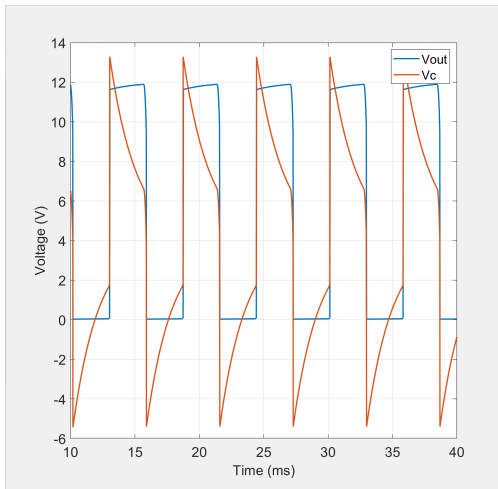


Fig. 22. Astable multivibrator as simulated.

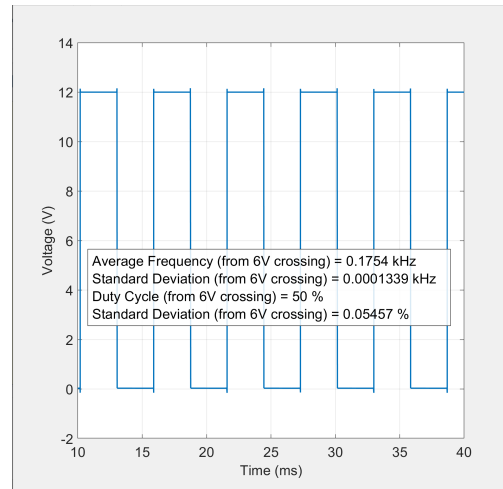
Because of this, the simulation parameters had to be very accurate to yield usable results. This was accomplished by first simulating the astable multivibrator with C_1 and C_2 equal to $0.1\mu\text{F}$.

3.2.1 Tuning the Simulation Results

Tuning the results was achieved by changing the V_{t0} value in CppSim/SpiceModels/2N7000_modified.SP3 to the measured value of 2.5V. The value was then adjusted until the simulation results matched the measured results in Section 4.2. The V_{t0} value set to 1.5V resulted in sub–figures 23a and 23b.



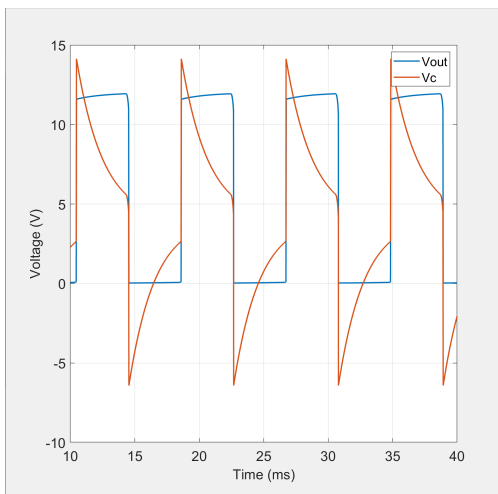
(a) Voltage across capacitor before V_{t0} was adjusted.



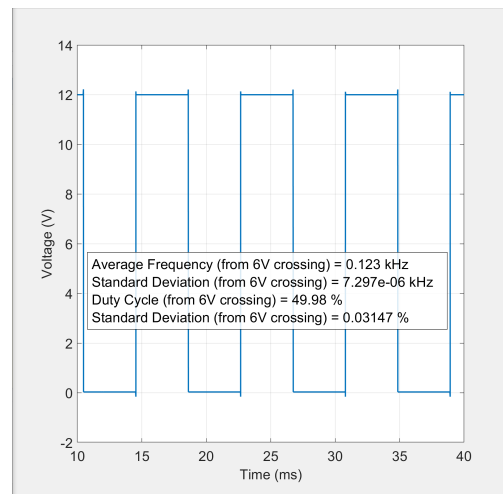
(b) Output voltage before V_{t0} was adjusted.

Fig. 23. Simulations run at C_1 and C_2 equal to $0.1\mu\text{F}$, before V_{t0} was adjusted.

The 175Hz seen in 23b is sufficiently close to the calculated value, 190Hz, only an 8% difference, which is acceptable for calculations. This made sense because the calculations assumed a 1.5V V_{t0} trigger voltage. Sub-figures 24a and 24b show the same simulations as sub-figures 23a and 23b, but with the V_{t0} value adjusted to 2.44V.



(a) Voltage across capacitor after V_{t0} was adjusted.



(b) Output voltage after V_{t0} was adjusted.

Fig. 24. Simulations run at C_1 and C_2 equal to $0.1\mu\text{F}$, after V_{t0} was adjusted.

The 128Hz simulated in Figure 24b sufficiently matched the measured values in Section 4.2, only varying by 3Hz or 2.5%. It was 38% different than the calculated value of 190Hz. However, as mentioned above, the calculated values assumed a V_{t0} of 1.5V. After the simulation was tuned, it could be used to determine a useful approximation of the capacitor values necessary to drive the boost converter.

3.2.2 Simulating the Final Circuit

After the capacitor values were confirmed, the final circuit was simulated again. This was done to further confirm the accuracy of the simulations. The values simulated and tested were not the same as determined in the boost converter lab, this is explained further in Section 5.2. Ultimately, it was the simulated and tested values that yielded 25V from the boost converter, not the expected values. Figure 25 shows the results of the final simulation.

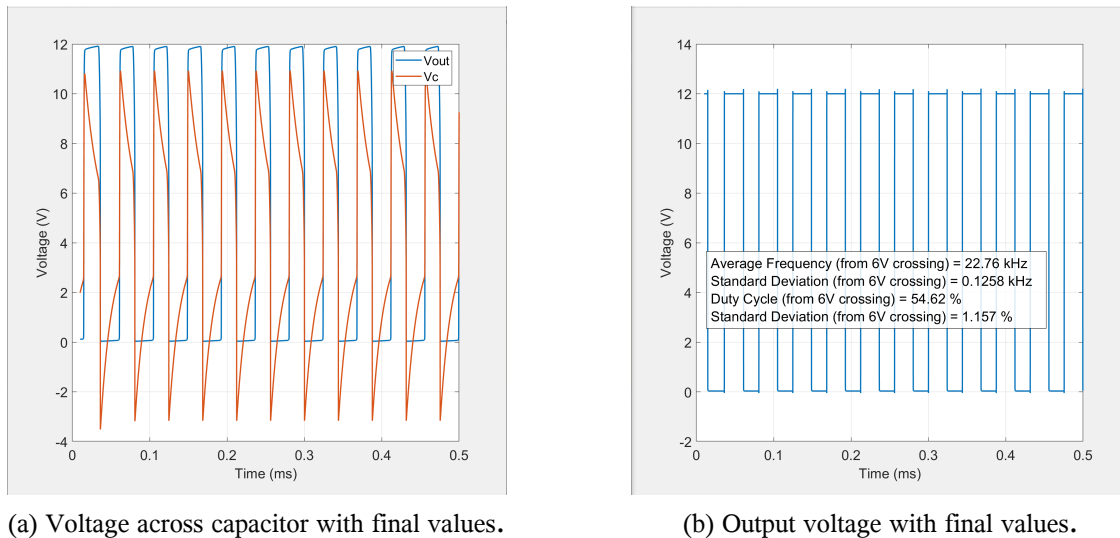
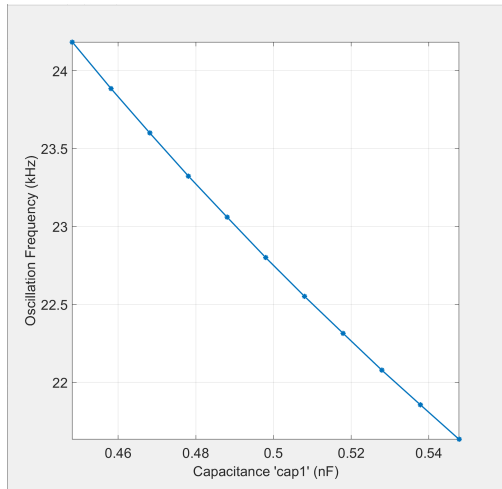


Fig. 25. Transient simulation run with final capacitor values C_1 equal to 498pF and C_2 equal to 706pF.

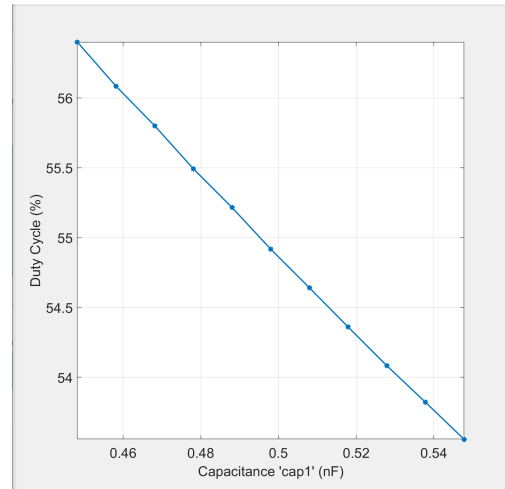
As can be seen in Figure 25, the frequency of 22.76kHz and duty cycle of 54.62% were within range of the measured values seen in Section 4.2.2. This meant the simulation has been adjusted correctly, and could be used to approximate capacitor values.

3.2.3 Capacitor and Resistor Sensitivity Analysis

Simulations were also run in order to determine appropriate tolerance values for each component in the astable multivibrator circuit. The capacitance of C_1 and C_2 were adjusted by $\pm 10\%$ at 2% increments. Figure 26 shows the first of these two sensitivity analyses.



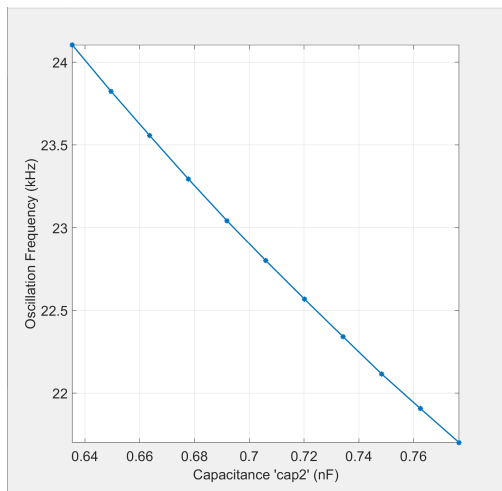
(a) Frequency sensitivity analysis run on C_1 .



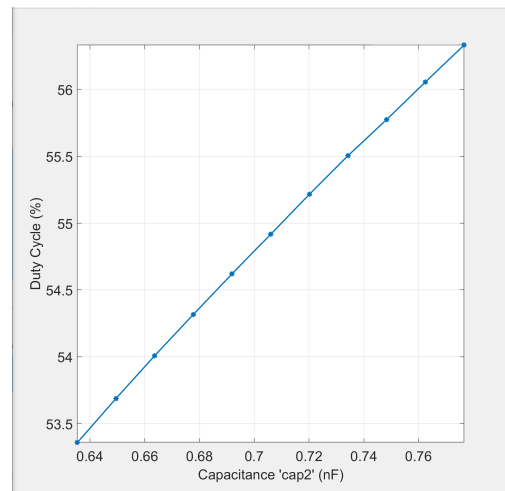
(b) Duty Cycle sensitivity analysis run on C_1 .

Fig. 26. Component sensitivity analysis simulations run for C_1 .

Figure 27 shows the second of these two sensitivity analyses, changing the capacitance of C_2 .



(a) Frequency sensitivity analysis run on C_2 .

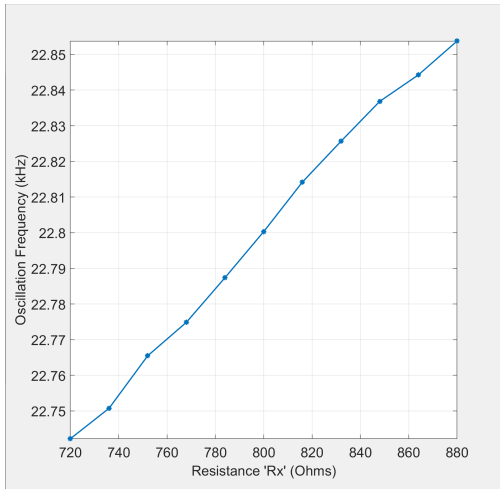


(b) Duty Cycle sensitivity analysis run on C_2 .

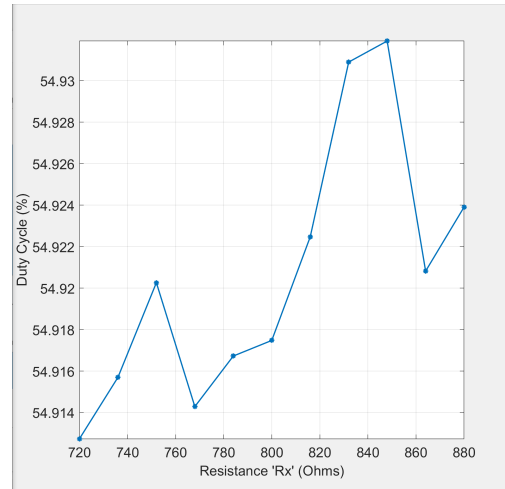
Fig. 27. Component sensitivity analysis simulations run for C_2 .

As can be seen in Figures 26 and 27, the frequency and duty cycle are moderately influenced by changes to C_1 and C_2 , changing by $\pm 1\text{kHz}$, and $\pm 3\%$ over the range. The duty cycle was affected more because it is directly related to the difference between the capacitors. Because of this influence, an appropriate tolerance for the capacitors was determined as $\pm 5\%$.

Next, the sensitivity of the resistors was investigated by also changing the resistances by $\pm 10\%$. For these figures, R_x is the 800Ω resistor, R_d is the $30\text{k}\Omega$ resistor, and R_u is the $60\text{k}\Omega$ resistor. Figure 28 shows the component sensitivity analysis for R_x .



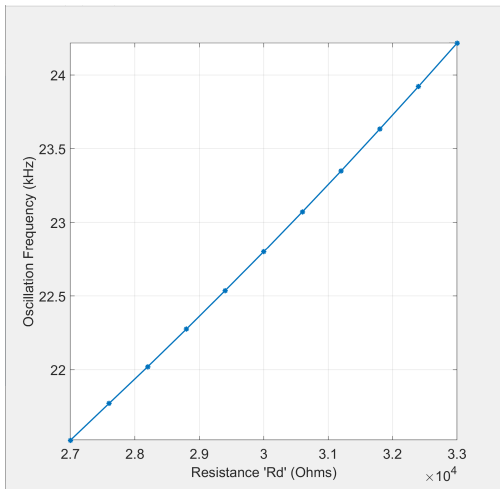
(a) Frequency sensitivity analysis run on R_x .



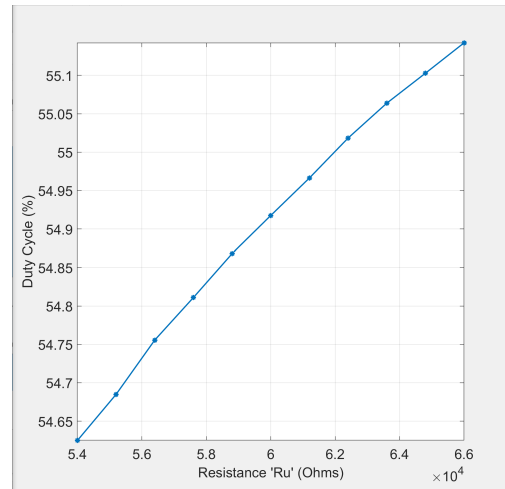
(b) Duty Cycle sensitivity analysis run on R_x .

Fig. 28. Component sensitivity analysis simulations ran for R_x .

As shown in Figure 28, the frequency and duty cycle do not change significantly with changes to R_x , only $\pm 0.05\text{kHz}$ and $\pm 0.1\%$. Because of this, the appropriate tolerance was increased to $\pm 10\%$. Figure 29 shows the component sensitivity analysis of R_d .



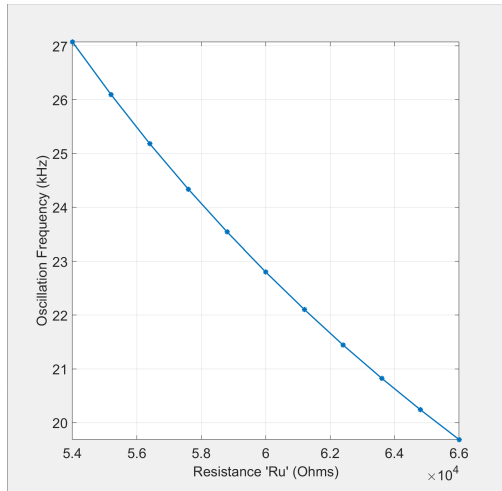
(a) Frequency sensitivity analysis run on R_d .



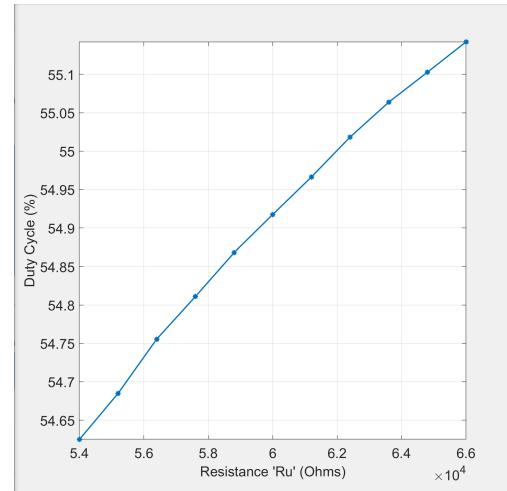
(b) Duty cycle sensitivity analysis run on R_d .

Fig. 29. Component sensitivity analysis simulations ran for R_d .

As seen in Figure 29, R_d affects the circuit in a similar way to C_1 and C_2 , $\pm 1\text{kHz}$ and $\pm 0.2\%$. Therefore the tolerance was determined to be $\pm 5\%$. Figure 30 shows the sensitivity analysis for R_u .



(a) Frequency sensitivity analysis run on R_u .



(b) Duty cycle sensitivity analysis run on R_u .

Fig. 30. Component sensitivity analysis simulations ran for R_u .

The effect of R_u on the multivibrator was more pronounced, especially on the frequency. The frequency varied by $\pm 3.5\text{kHz}$, while the duty cycle varied by $\pm .3\%$. Because of this, the appropriate tolerance was reduced to $\pm 1\%$.

3.3 DC–DC Power Supply Simulation

The values used to simulate the DC–DC power supply in this section are the same as the final values because the simulations and measurements were used together to determine the correct values. Figure 31 shows the full DC–DC power supply circuit simulated to check if the low pass filter would work properly.

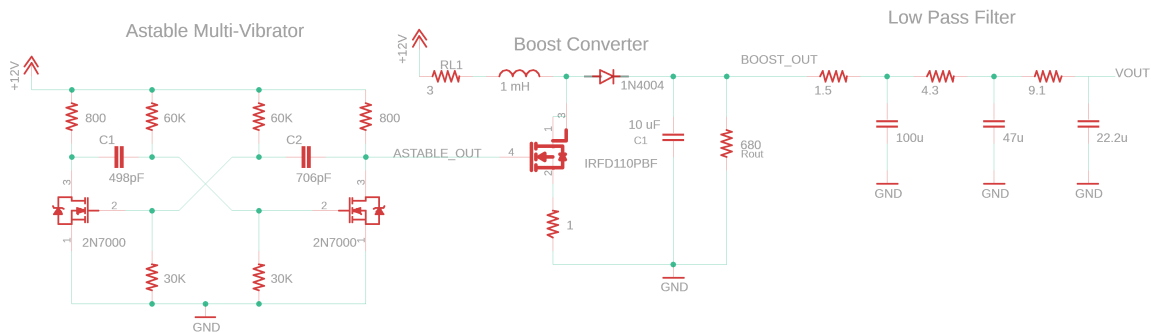
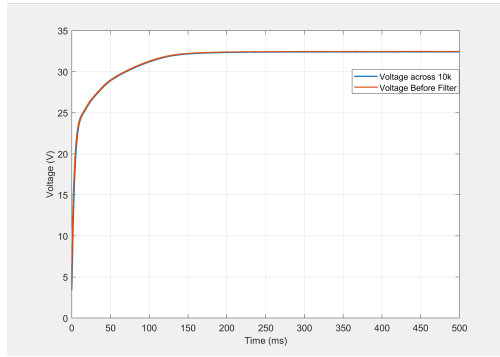
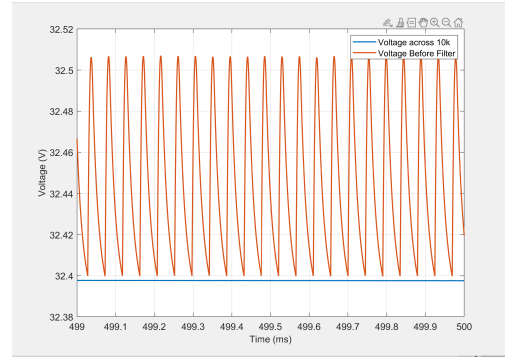


Fig. 31. Power supply circuit as simulated.

The low pass filter was not simulated independently because it made more sense to simulate the full power supply. Specifically, the output of the boost converter needed to be attenuated, so the whole supply was simulated. Figure 32 shows the full length, and steady state simulations of the power supply.



(a) Full simulation of the power supply.



(b) Steady state simulation of the power supply.

Fig. 32. Transient Analysis Simulations of the DC–DC power supply.

As can be seen in Figure 32a, the voltage was simulated to be almost 32V. This did not match measurements, and the error was predicted to be from the boost converter part of the simulation, more discussion into this error is in Section 5.4. Ultimately, the voltage reading was only used to confirm that the voltage across the 10kΩ would not be significantly less than the voltage before the filter. As can be seen in Figure 32b, the voltage drop before and after the filter was small enough to retain 25V at output, and the AC ripple is 100μV.

4 Experimental Implementation

Figure 33 shows the full power supply schematic as measured, with real values.

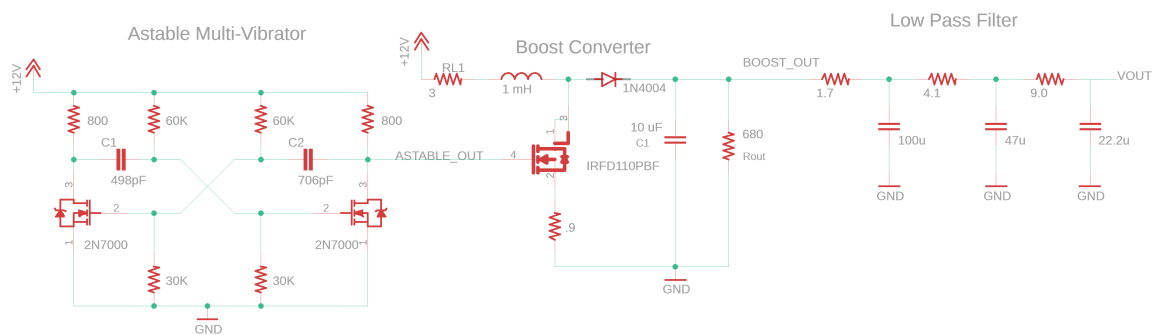


Fig. 33. Final schematic of DC–DC power supply, as measured.

The DC–DC Power Supply was built using the designs as finalized in Section 3. All constructions were performed on a standard breadboard. The 12V source was provided by a Digilent 12V PowerBRICK. Measurements were taken using the oscilloscope features of the Digilent Analog Discovery 2 (AD2). The AD2 waveform generator was also used to drive V_{FG} . For DC voltages, a Digital Volt Meter (DVM) (Neoteck NT8233D Pro) was used. Measurements were taken primarily to confirm results were within

circuit specifications. However, they were also used to confirm the accuracy of the astable multivibrator simulations. Sections 4.1, 4.2, and 4.3 discuss the measurement process for the boost converter, astable multivibrator, and full DC–DC power supply, respectively.

4.1 Boost Converter

The final design schematic of the boost converter can be seen in Figure 34. Here, R_0 is implemented by a 3x3 680 Ω resistor bank to sufficiently dissipate power. At first, a 2x2 bank was used, but the resistors started to heat up too much, so it had to be expanded. In the 3x3 configuration, the resistor bank should be able to handle 2.25W of power, which is well above the calculated 0.9W.

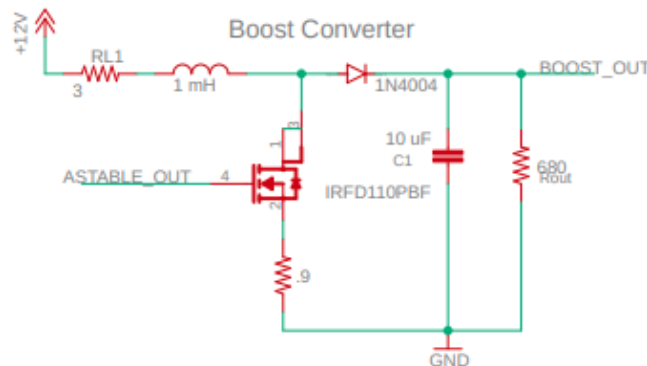


Fig. 34. Final schematic of boost converter circuit.

V_{FG} was driven by the AD2's Waveform Pulse Generator with the previously defined period equal to 40 μ s and a slightly adjusted duty cycle of 56.5%. The duty cycle needed to be adjusted for V_{out} to be 25V DC. An oscilloscope probe was placed across the 1 Ω resistor (Channel 1), across the 10 μ F capacitor (Channel 2), and the DVM was placed across the capacitor as well. The measurements as observed in the WaveForms software can be seen in Figure 35.

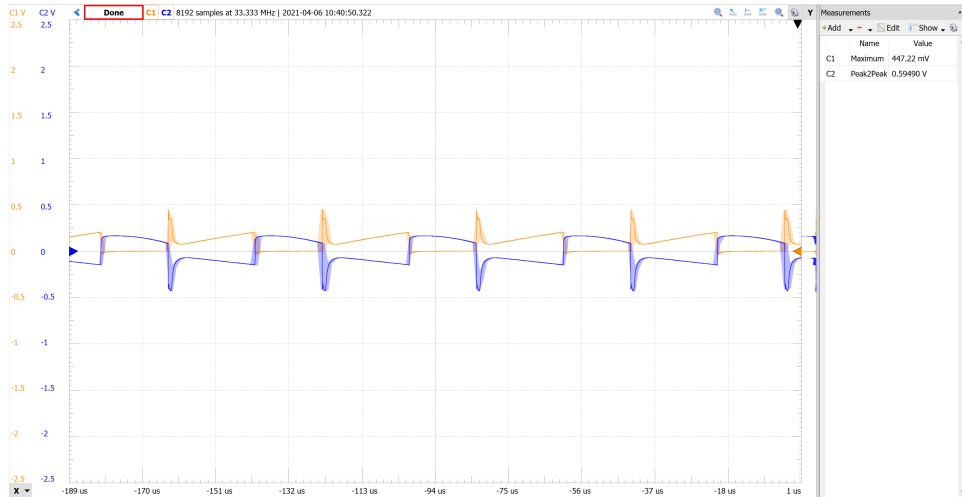


Fig. 35. Measurements of boost converter circuit.

Here Channel 1 and Channel 2 are abbreviated as C1 and C2 respectively. As can be seen in Figure 35, the measured AC Ripple was higher than simulated, but there was no AC ripple specification for this circuit. The DVM can be seen reading 25.0V DC in Figure 36, which is within the specification of $25 \pm 0.25V$.

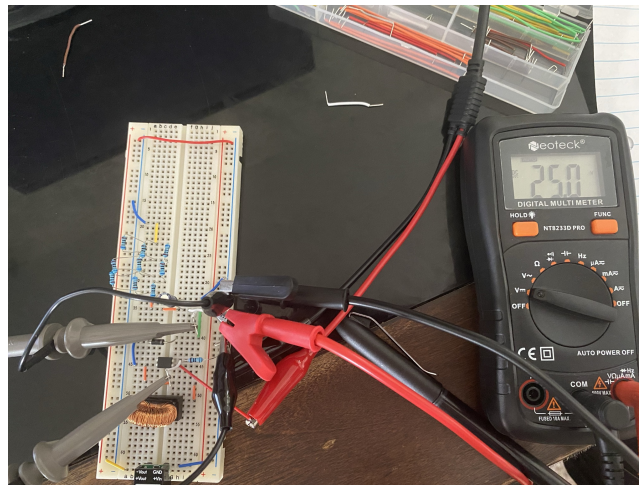


Fig. 36. Picture of the circuit including DVM measurements.

As can be seen in Figure 36, the circuit operates as expected.

4.2 Astable Multivibrator

The astable multivibrator shown in Figure 37 was measured with two different sets of capacitor values. Initially, values were set to $0.1 \mu F$ in order to tune the simulation results as detailed in Section 3.2. Then,

the values were changed to C_1 equalling 498pF and C_2 equalling 706pF, in order to produce the necessary frequency and duty cycle to drive the boost converter.

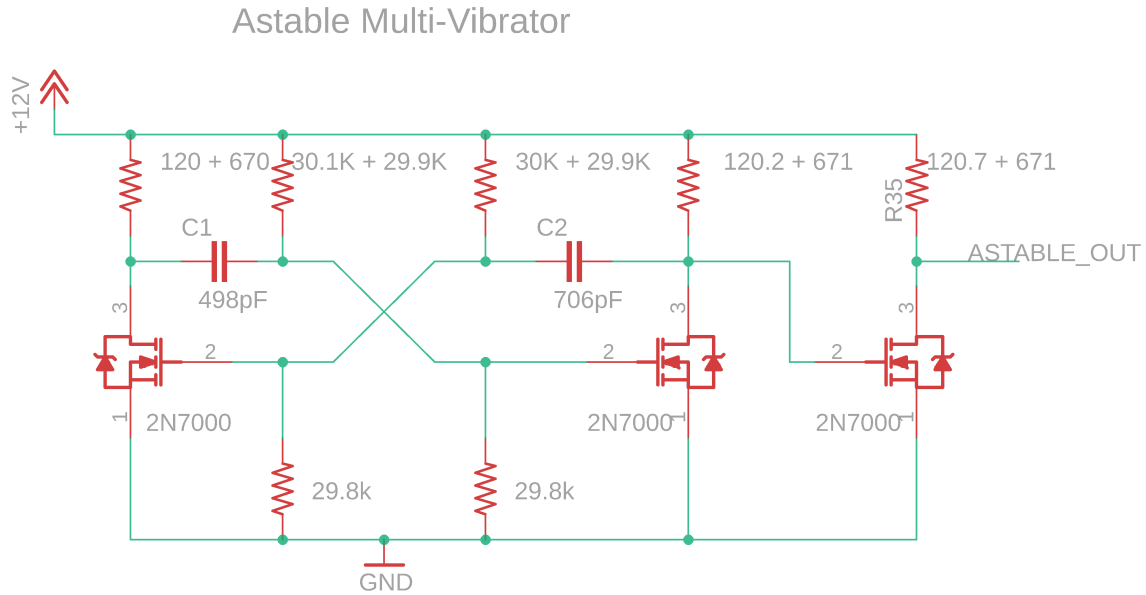


Fig. 37. Astable Multivibrator as measured.

4.2.1 Determining 2N7000 Trigger Voltage

V_{t0} , the trigger value of the 2N7000 transistors, had to be determined in order to adjust the value used in simulations, as described in Section 3.2. This value was measured by inserting one 2N7000 at a time in the half circuit depicted in Figure 38.

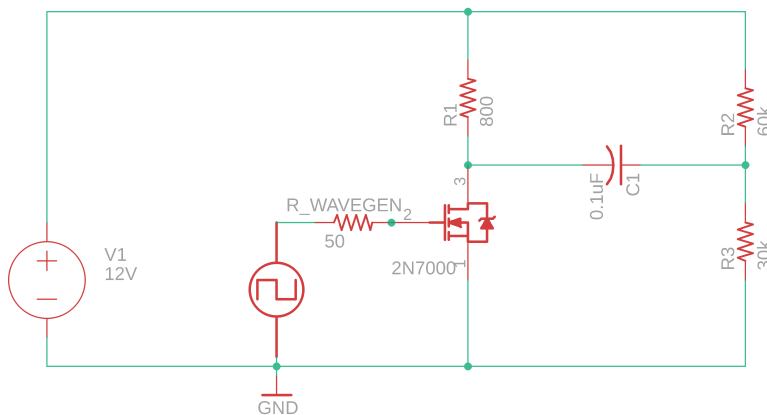


Fig. 38. Astable Multivibrator half circuit.

V_{FG} was driven by the AD2 Waveform Generator producing a 0 to 5V pulse at a frequency of 190Hz.

When measuring across the drain (d) and gate (g) of the 2N7000, the trigger voltage was found when the two voltages cross paths. As seen in Figures 39a, 39b, and 40, the crossing appears to be at 2.5V. This was initially questioned as it was much higher than the expected 1.5V. Because of this skepticism, measurements were taken when the C1 voltage started to decrease, instead of at the crossing. However, later simulations confirmed the 2.5V value to be accurate. The enumeration of transistors is defined by left-to-right reading of the schematic, i.e. the leftmost transistor is transistor 1.

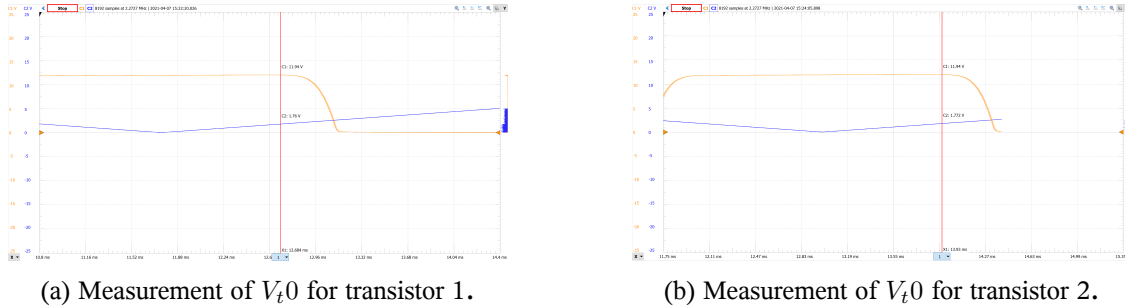


Fig. 39. Measurement of V_{t0} for transistors 1 and 2.

The third transistor was used for filtering the output of the circuit, because there was capacitance on the ideally square wave output signal. The V_{t0} measurement was can be seen in Figure 40.



Fig. 40. Measurement of V_{t0} for transistor 3.

Lastly, a measurement of the frequency of the circuit with C_1 and C_2 equal to $0.1\mu\text{F}$ was taken. This measurement was taken so V_{t0} could be changed until the simulation of the circuits frequency $0.1\mu\text{F}$ capacitors matched the measurements taken. Figure 41 shows these measurements.

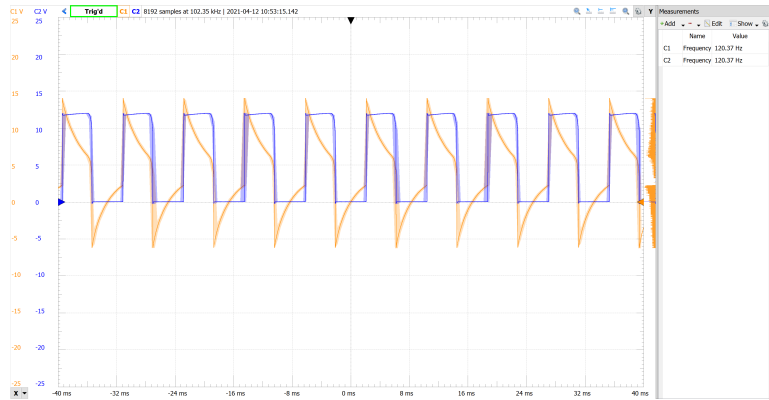


Fig. 41. Measurement of Frequency with C_1 and C_2 equal to $0.1\mu F$.

4.2.2 Driving the Boost Converter

The ultimate goal of the astable multivibrator is to provide a signal to the IRFD110 in the boost converter. To accomplish this, it was expected that a signal at 25kHz, 56.5% duty cycle would be needed. The actual values that worked were significantly different from expected. Ultimately, as can be seen in Figure 42, the frequency was 22.864 khz and 53.6% duty cycle. In Figure 42, C1 is the output of the astable multivibrator and C2 is the voltage across the capacitor in the boost converter. It can be seen that the voltage across the capacitor has an average value of 25.029V, which is within specifications.



Fig. 42. Measurements taken of combined boost converter and astable multivibrator circuits.

To further confirm the boost converter was being properly driven, the voltage across the output capacitor was measured using the DVM. A photo of that measurement can be seen in Figure 43.

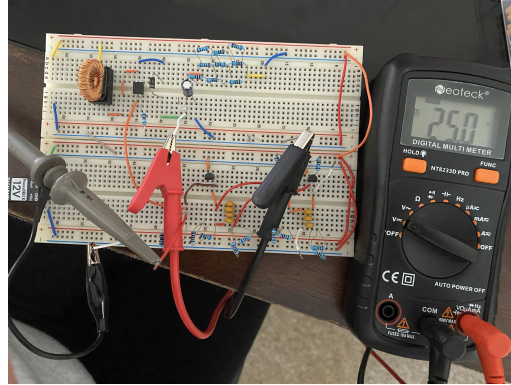


Fig. 43. Photo of combined boost converter and astable multivibrator circuits.

As seen in Figure 43 the two circuits were connected together, and a steady 25.0V DC was read by the DVM across the boost converter output.

4.2.3 Checking the IRFD110 Transistor

Because the IRFD110 MOSFET in the boost converter has a max listed current, the current through this transistor was also measured with the astable multivibrator driving the circuit instead of the AD2 waveform generator. The findings of this measurement can be seen in Figure 44.

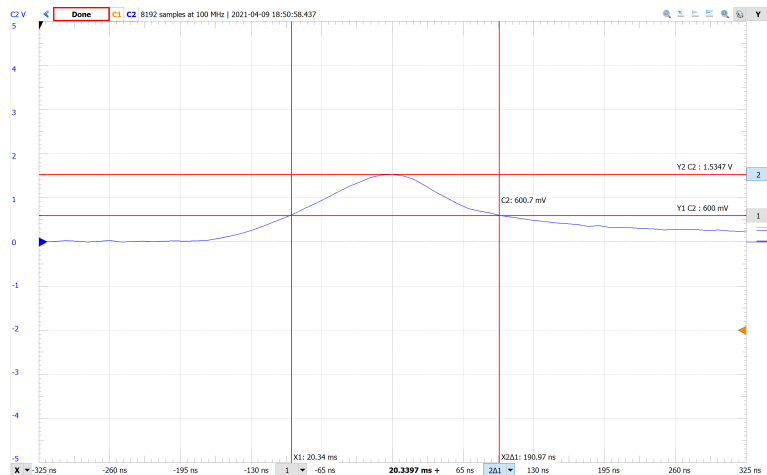


Fig. 44. Measurement taken across the 1Ω resistor in the boost converter circuit.

As can be seen in Figure 44, the current does exceed the 600mA max limit, reaching 1.5A. However, it is only above the 600mA limit for 190ns, therefore it does no damage to the part, and the circuit works as expected.

4.3 DC–DC Power Supply

Figure 45 shows the full power supply circuit as measured.

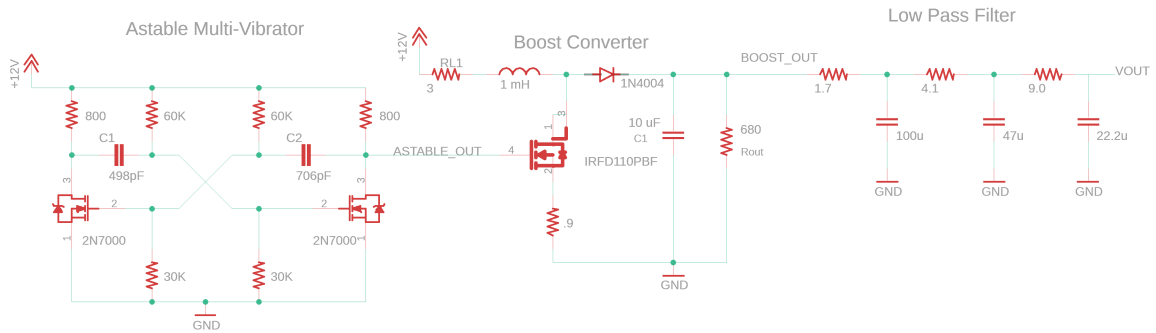


Fig. 45. Final schematic of DC–DC power supply, as measured.

Here, the final values were measured, which are as follows: R_1 , R_2 , and R_3 equal to 1.5Ω , 4.3Ω , and 9.1Ω . Figure 45 shows the measured component values. Similar to Section 3.3, the low pass filter was not measured independently. Instead, the whole DC–DC power supply was built and measured. The reduction of ripple was the primary objective for the low pass filter. Therefore, Channel 1 of the oscilloscope was set to AC coupling and the voltage across the $10k\Omega$ resistive load was measured. The DVM was also used to confirm the DC output voltage across the same load resistor. Figure 46 shows the ripple as measured in Waveforms.

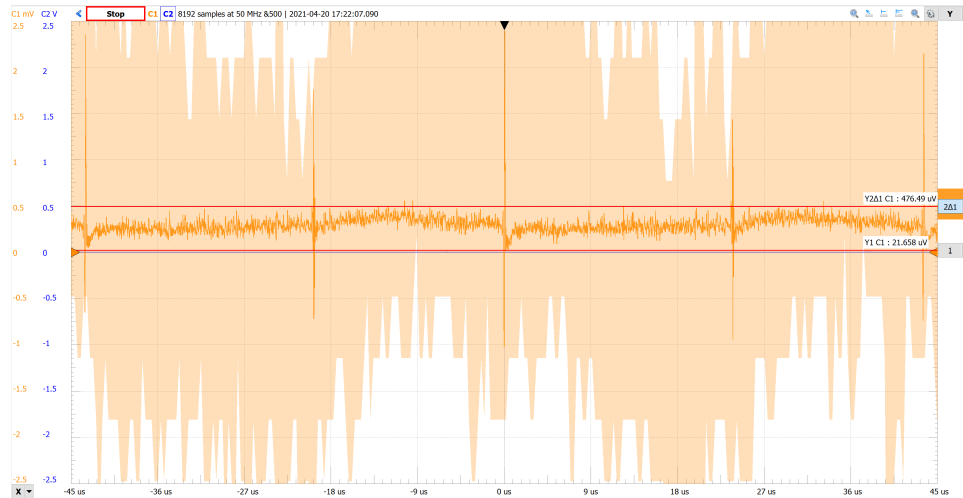


Fig. 46. Measurement of AC ripple across the load resistor.

In order to get clean results, averaging was set to 500, and the scale was set to $500\mu\text{V}$ per division. As can be seen, the peak to peak ripple measured $476.49\mu\text{V}$, which is below the $.5\text{mV}_{\text{PP}}$ specification. Figure 47 shows a photo of the DC–DC power supply fully built with the DVM measuring across the load resistor.

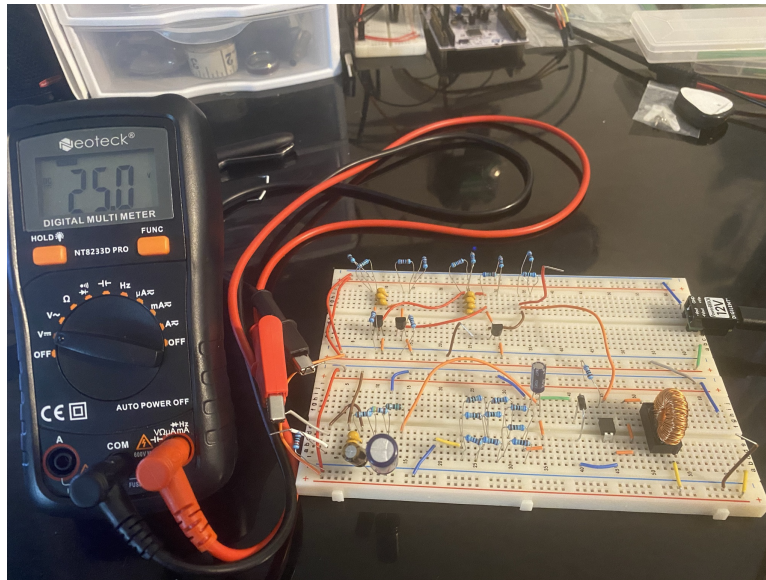


Fig. 47. Photo of DVM measuring across the load resistor.

As can be seen, the DVM read 25.0V across the load resistor, meaning the power supply performs within the $25.0 \pm 0.25\text{V}$ specification.

5 Discussion

The power supply worked as expected, although there were plenty of adjustments needed to get the proper output. Calculations were often within 10% of the simulated values, which in turn were often within 5% of the measured values. Appendix A includes Table VI, which is a Bill of Materials for the power supply circuit. This table was populated with the components used in each lab, not the ideal components. For example, the number of $680\Omega \pm 1\%$ resistors could be reduced if 2W resistors were available. If they were, one resistor would have been sufficient to safely dissipate power in the boost converter. Additionally, the tolerance values are based off the actual components. A detailed analysis of the necessary component sensitivities for the astable multivibrator can be found in Section 3.2.3. The ceramic capacitors used in the power supply did not list their tolerances, so they were assumed to be 10%. Other sources of error could have arisen from less than ideal measuring equipment, and sub-optimal breadboard design. The DVM used was not capable of measuring capacitor values, therefore the true capacitance of the capacitors used is unknown. The DVM also only showed 3 significant figures, so the precision of the measurements were limited. Additionally, it was observed that tapping the resistors in the output resistor bank could cause the voltage to vary by almost 0.2V. This is likely due to the resistors being in close proximity to each other in the breadboard and making contact, causing the resistor bank equivalent resistance to change slightly. Lastly, many jumpers were used in the breadboard construction, which may have introduced parasitic capacitance between the jumpers and the breadboard contacts. The circuit could have been built with less jumpers, but they proved useful for troubleshooting during construction. Sections 5.1, 5.2, 5.3, and 5.4 discuss the boost converter, astable multivibrator, and full DC-DC power supply in more depth.

5.1 Boost Converter

The boost converter implementation was relatively straightforward. The final boost converter met the $25 \pm 0.25\text{V}$ DC specification. The ripple was out of spec, but it was later reduced by the low pass filter. The steady state output on the DVM was 25.0V DC and the current was safe for the transistor in all simulations and the measurements. Values had to be changed in each stage in order to continue to meet requirements, the comparison of these values can be seen in Table I.

TABLE I
Boost converter comparisons.

Stage	$t_1(\mu\text{s})$	$t_2(\mu\text{s})$	$R_0(\Omega)$	$\delta(\%)$	V_{out} (V DC)	AC ripple (V_{ptp})
Calculated	18.58	16.6	680	52.8	25	Not Calculated
Simulated	21.9	18.1	680	54.75	25	.0989
Measured	22.5	17.5	680	56.25	25	.59490
Specifications	–	–	–	–	25	.5 μ

As mentioned in Section 4, the AC ripple was higher than simulated, but that was a nonissue for this circuit, as the low pass filter later reduces it. The only large adjustment that was made for the boost converter was to the output resistor. As mentioned in Section 2.1.4, the resistors had to be changed to a larger value to safely handle the power output of .9W. A 2x2 resistor bank was initially used, which theoretically could handle 1W, but the resistors got too hot, and therefore a 3x3 was used. As mentioned before, 2W resistors would have been ideal for the output resistor.

As can be seen in Table I, the expected values were close to the actual results. Most of the changes made were small, and only done to get the results to match the specifications exactly. For example, a voltage of 24.9V was not acceptable, values were changed until 25.0V was read. Also, the DC output met specifications, but the AC ripple did not. The ripple was later reduced with the low pass filter discussed in Section 5.3

5.2 Astable Multivibrator

The astable multivibrator had more issues in its implementation than the boost converter. Due to a combination of adequately accurate simulations and measurements were used to determine the correct capacitor values. In order to achieve the boost converter specifications, capacitor values were swapped multiple times. Ultimately, the frequency and duty cycle that yielded results within specifications were lower than expected, at 22.864kHz , and 53.6% . When a signal of 25kHz and duty cycle of 57% (the expected values) was used to drive the boost converter, 26.5V was measured on the DVM. This was likely caused by the different input impedances of the astable multivibrator and the AD2 waveform generator. Additionally, the output resistor bank was noticeably warmer compared to when the AD2 drove the circuit. The temperature was not unsafe, but was still noticeable. Ideally, the circuit would use 2W resistors for the output, allowing more power and therefore heat dissipation, but only $1/4\text{W}$ resistors were available. Table II shows the results of each stage of the experiment.

TABLE II
Astable multivibrator comparisons.

Stage	Frequency(kHz)	Positive Duty Cycle (%)
Calculated	.190	Not Calculated
Simulated (0.1 μ F before V_i0 change)	.175	50
Simulated (0.1 μ F after V_i0 change)	.123	49.98
Simulated (498pF and 706pf)	22.76	54.62
Measured (0.1 μ F)	.120	Not Measured
Measured (498pF and 706pf)	22.864	53.6

Tuning the simulation saved time that would have been spent testing random capacitor values. Because it gave accurate results, much of the testing of values came by repeating simulation runs, rather than replacing physical capacitors. Ultimately, the circuit performed as expected, the boost converter, when driven by the astable multivibrator outputs 25V DC.

5.3 Low Pass Filter

Implementation of the low pass filter was similar to the astable multivibrator. The simulations and calculation were used to determine an appropriate estimate for the resistor and capacitor values in the low pass filter. This resulted in a long series of running simulations and testing components in the circuit to find the appropriate values. The speed of this process was increased when it was noticed that larger, greater than 10 μ F, would be needed. Once the large capacitor values were determined the resistors were only changed slightly from calculated values to get correct results. Table III shows the values of the low pass filter at each stage of the implementation.

TABLE III
Low pass filter comparisons.

Stage	$R_1(\Omega)$	$R_2(\Omega)$	$R_3(\Omega)$	$C_1(\mu F)$	$C_2(\mu F)$	$C_3(\mu F)$	$f_{c1}(\text{Hz})$	$f_{c2}(\text{Hz})$	$f_{c3}(\text{Hz})$
Calculated	3.3	6.2	12	100	47	22.2	482	546	597
Simulated	1.5	4.3	9.1	100	47	22.2	1061.0	787.5	787.8
Measured	1.7	4.1	9.0	100	47	22.2	936.2	825.9	796.5

As can be seen, values for the resistors and capacitors did not require large adjustments between calculated and simulated. The measured values shown in the table are the real values of the value simulated. Ultimately, it was found that a higher cutoff frequency was needed to yield correct results.

5.4 DC–DC Power Supply

Because the low pass filter was simulated as part of the larger power supply circuit, building the DC–DC power supply simply required connecting the boost converter, astable multivibrator, and low pass filter together. Each circuit built off the previous ones so these connections were already determined and made. Table IV shows the predicted and actual values of the output voltage and AC ripple of the full power supply.

TABLE IV
DC–DC power supply comparisons

Stage	DC Voltage (V)	AC ripple(μV_{PP})
Simulated	32.4	100
Measured	25.0	476.49
Specifications	25.0 ± 0.25	<500

There is clearly a large difference between the expected and measured values. This error has multiple explanations. The first and most likely, the simulated values were ideal, and measured were real. Second, the AC ripple was a very small value, so the accuracy of the AD2 oscilloscope probes were questioned. Peers observed significant AC noise present in the AD2. Luckily, the AD2 used in this report did not have enough AC noise to increase the ripple above the specified $.5\text{mV}_{\text{PP}}$. However, it could have increased the change between simulated and expected results. The DC voltage change can be explained by the boost converter simulations. The simulation method used produced accurate results when the values for frequency and duty cycle were 25kHz and 56.5%, respectively. When the full power supply was simulated, it used the astable multivibrator simulation to drive the boost converter. Because the astable multivibrator was adjusted to reflect real world measurements (as detailed in Section 3.2.1), it produced the values found in Section 3.2.2. Specifically, 22.76kHz and 54.62%. Because of this, the simulated boost converter produced a much higher voltage than measured. Ultimately, the simulated voltage was used to observe the change between the voltage before and after the filter. Ultimately, the DC–DC power supply circuit performed as expected. As can be seen in the 3rd row of Table IV, the measured values of 25.0V DC and $476.49\mu\text{V}_{\text{PP}}$ are within the $25.0 \pm 0.25\text{V}$ DC and $.5\text{mV}_{\text{PP}}$ specified.

6 DC–DC Power Supply Cost Estimate

When manufacturing a device at cost there are many aspects of the process that affect the price: components, printed circuit board (PCB) size, engineering/design costs, testing, yield, after–sale support, and profit margin.

If you were to add up the raw cost of the components (Appendix A) it would come out to \$3.72. It should be noted that this value is not including the cost of the Digilent PowerBRICK as this is used for prototyping and does not belong in the final design, nor the cost of manufacturing. The raw cost is calculated using resistors combinations to achieve a goal resistance, or multiple are used to create a resistor bank in order

to handle high wattage – this is a product of the prototyping process – at scale the resistor combinations will be switched with resistors matching the goal resistance and power limits. Currently the board has 25 resistors on it (50 leads), about half of them are used in a combination, if these were switched with better fitting resistors about \$0.25 will be taken off the price before, bringing it to \$3.47 (not including manufacturing).

Manufacturing costs with the parts in Appendix A could increase the price significantly, as through hole manufacturing has more human intervention (lead bending, hand soldering). Assuming each connection is \$0.005, the assembly cost will come to \$0.37. However, if surface mount components were to be used instead the PCB can be manufactured efficiently in a pick and place machine. Using surface mount technology will also make a physically smaller PCB, reducing cost. However, without these cost reducing measures, the full cost of manufacturing and assembly is \$4.09 per unit. Once yield at 95% is taken into account, this figure is increased by 5% to cover cost of reworks, increasing the cost to \$4.29. Next, testing must be conducted. Testing would be conducted by a technician, taking into account salary, benefits, and overhead results in \$50/hour, or \$0.83/unit. The production cost is now \$5.12/unit, after sale support and maintenance would add another 2% to the cost, resulting in a final cost of \$5.22/unit, yielding \$52, 224 for 10,000 units.

For this project, approximately 50 design ours were spent – this includes initial calculations, simulations and prototyping. For estimations sake, a professional engineer would do it in 60% of the time – 30 hours, which at an average salary of \$85, 000 yields \$42.50/hour. Once overhead costs are taken into account, the cost per hour is increased to \$110.00/hour. This results in a total design cost of \$3, 300. Adding this design cost to the manufacturing and assembly cost for 10,000 units results in an expense total of \$55, 524.00. Finally, a profit margin must be added. This was decided to be 15%. With the profit margin added, the total cost increases to \$63, 407, resulting in a final sales price of \$6.34 per unit. Table V shows an itemized breakdown of the power supply cost estimate.

TABLE V
DC–DC power supply cost estimate

Item	Per Unit cost (\$)	Total cost (10,000 units) (\$)
Components	3.72	37,200
Assembly	0.37	3,700
Yield coverage (5% of above items)	0.20	2,000
Testing (\$50/hr)	0.83	8,300
After–sale support (2% of above items)	0.10	1,000
Engineering/Design (\$110/hr at 30hrs)	0.33	3,300
Profit Margin (15%)	0.79	7,983
Final Cost	6.34	63,407

7 Conclusions

In this lab, a DC–DC power supply was designed. A boost converter and astable multivibrator are powered by a 12V DC input. The astable multivibrator then produced a square wave that controlled the boost converter output voltage, producing 25V DC. The output of the boost converter is then filtered through a third order RC low pass filter that attenuated the AC ripple riding on the DC signal. The DC–DC power supply operated as intended. When a 12V DC source was fed into the power supply, it outputted 25V DC across a 10k resistive load, with a ripple of 476.49mV_{pp}. These measurements are within the given specifications of 25 ± 0.25 V DC and less than 0.5mV_{pp}.

Appendices

Appendix A Bill of Materials

TABLE VI
Bill of materials for 1 DC-DC power supply.

Item	Part No.	Description	Qty.	Unit Price (\$)	Total Leads
1	RNMF14FAD680RCT-ND	RES 680 OHM 1/4W 1% AXIAL	12	0.01100	24
2	S120CACT-ND	RES 120 OHM 1/4W 1% AXIAL	3	0.00855	6
3	S30KCACT-ND	RES 30K OHM 1/4W 1% AXIAL	6	0.00855	12
4	RNF14FAC1R00-ND	RES 1 OHM 1/4W 1% AXIAL	1	0.00475	2
5	RNF14FTD1R50-ND	RES 1.5 OHM 1/4W 1% AXIAL	1	0.01500	2
6	MFR25SFRF52-4R3-ND	RES 4.3 1/4W 1% AXIAL	1	0.01875	2
7	MFR25SFTF52-9R1-ND	RES 9.1 1/4W 1% AXIAL	1	0.01875	2
8	399-6599-ND	CAP ALUM 10UF 20% 50V RADIAL	3	0.03920	6
9	1242PH-ND	CAP CER 330PF 1KV Y5R RADIAL	2	0.06999	4
10	BC5224CT-ND	CAP CER 100PF 50V C0G/NP0 RADIAL	2	0.05111	4
11	BC2672CT-ND	CAP CER 220PF 50V X7R RADIAL	1	0.03871	2
12	K680J10C0GF5TH5-ND	CAP CER 68PF 50V C0G/NP0 RADIAL	1	0.03188	2
13	K560J10C0GF5UH5-ND	CAP CER 56PF 50V C0G/NP0 RADIAL	1	0.03188	2
14	399-6105-ND	CAP ALUM 100UF 20% 50V RADIAL	1	0.08791	2
15	493-15143-ND	CAP ALUM 47UF 20% 50V RADIAL	1	0.07232	2
16	RDEC71H106K3M1H03A-ND	CAP CER 10UF 50V X7S RADIAL	1	0.52519	2
17	811-1217-ND	FIXED IND 1MH 450MA 568 MOHM TH	1	1.35660	4
18	12-1N4004GPE-E3/54CT-ND	Diode Standard 1A DO-204AL	1	0.13939	2
19	IRFD110-ND	MOSFET N-CH 100V 1A 4DIP	1	0.53000	4
20	1286-1106-ND	DC DC CONVERTER +/-12V 2W	1	19.110	4
21	2N7000FS-ND	MOSFET N-CH 60V 200MA TO92-3	3	0.12791	9

References

- [1] D. E. Kotecki, "ECE 214 – electrical circuits laboratory: Laboratory #9," 2021. [Online]. Available: http://davidkotecki.com/ECE214/labs/ECE214_2021_Lab9.pdf